Chamber simulation on the formation of secondary organic aerosols (SOA) from diesel vehicle exhaust in China

Wei Deng[1,2], Qihou Hu[1], Tengyu Liu[1,2], Xinming Wang[1,*], Yanli Zhang[1], Xiang Ding[1], Yele Sun[3], Xinhui Bi[1], Jianzhen Yu[4], Weiqiang Yang[1,2], Xinyu Huang[1,2], Zhou Zhang[1,2], Zhonghui Huang[1,2], Quanfu He[1,2], A. Mellouki[5], Christian George[6]

[1]State Key Laboratory of Organic Geochemistry and Guangdong Key Laboratory of Environmental Protection and Resources Utilization, Guangzhou Institute of Geochemistry, Chinese Academy of Sciences, Guangzhou 510640, China

[2]University of Chinese Academy of Sciences, Beijing 100049, China

[3]Institute of Atmospheric Physics, Chinese Academy of Sciences, Beijing 100029, China

[4]Division of Environment, Hong Kong University of Science & Technology, Clear Water Bay, Kowloon, Hong Kong, China

[5]Institut de Combustion, Aérothermique, Réactivité et Environnement (ICARE), CNRS, 45071 Orléans cedex 02, France

[6]Institut de Recherches sur la Catalyse et l'Environnement de Lyon (IRCELYON), CNRS, UMR5256, Villeurbanne F-69626, France

*Corresponding author:

Dr. Xinming Wang

State Key Laboratory of Organic Geochemistry

Guangzhou Institute of Geochemistry, Chinese Academy of Sciences

Tel: +86-20-85290180; Fax: +86-20-85290706

Email: wangxm@gig.ac.cn

Abstract

In China primary particulate matter emission from on-road vehicles is predominantly coming from diesel, yet secondary organic aerosol (SOA) formed from diesel emission may be also of greater significance due to more intermediate volatile organic compounds (IVOC) in the exhaust. Here exhaust from three in-use diesel vehicles under warm idling condition was directly added into an indoor smog chamber with a 30m^3 Teflon reactor. The SOA formation as well as chemical aging of organic aerosols during photo-oxidation was investigated. The emission factors of primary organic aerosol (POA) and black carbon (BC) for the three typical Chinese diesel vehicles ranged 0.18-0.91 and 0.15-0.51 g kg-$fuel^{-1}$, respectively; and the SOA production factors ranged 0.50-1.8 g kg-$fuel^{-1}$ with an average SOA/POA ratio of 1.6, lower than ratios of ~3 reported in previous studies for diesel exhaust in USA or Europe. Aromatic hydrocarbons could only explain less than 3% of SOA formed during aging. The heterogeneous reaction of gas-phase oxidation products (like glyoxal and methylglyoxal) and the degradation of IVOC and semi-VOC (like PAHs) in the particulate phase might contribute substantially to the SOA formation. High resolution time-of-flight aerosol mass spectrometer (HR-ToF-AMS) resolved that POA had higher O/C ratios with less volatility than those in previous studies in USA or Europe, which could partly explain the lower SOA/POA ratios observed. During the photo-oxidation, the slopes of O/C versus H/C element ratios in the Van Krevelen diagram ranged from -0.47 to -0.68, suggesting a combination of carboxylic acid and alcohols/peroxides formed during the aging of diesel exhaust.

1 Introduction

Air pollution by particulate matter not only adversely affects human health by causing respiratory and cardiopulmonary diseases (Pope et al., 2009; Brook et al., 2010; Liu et al., 2015b; Lelieveld et al., 2015), but also impacts regional and global climate (Ramanathan et al., 2001; Parrish and Zhu, 2009; Wang et al., 2014b). Health risks are of particular concern when heavy fine particle (particulate matter with dynamic diameter less than 2.5 μm, $PM_{2.5}$) pollution occurs in densely populated megacities, such as China's capital city Beijing, which is hard-hit by frequent heavy haze episodes with a large body of people exposed to severe $PM_{2.5}$ pollution (Guo et al., 2014; Huang et al., 2014). In urban agglomerations, vehicle exhaust contributes substantially to $PM_{2.5}$, with mass fractions ranging from ~22% in southeastern US (Chen et al., 2012), ~37% in Guangzhou in the Pearl River Delta during wet season (Cui et al., 2015), to as high as 49% in Mexico City (Stone et al., 2008). In particular, People usually expose to much higher air pollutants in urban roadside microenvironments due to traffic-related emission (Zhao et al., 2004; Xu et al., 2008). Nevertheless, the contribution of vehicle exhaust to $PM_{2.5}$ is often a debatable issue. In Beijing, for example, previous studies revealed that contributions of vehicle exhaust to $PM_{2.5}$ ranged from 4% to 16.3% (Zheng et al., 2005; Song et al., 2006a, b, 2007b; Zhang et al., 2013; Wu et al., 2014), whilst very recently Beijing Municipal Environmental Protection Bureau announced that vehicle exhaust alone accounted for 31% of $PM_{2.5}$ mass (http://www.bjepb.gov.cn/bjepb/413526/331443/331937/333896/396191/index.html). One crucial reason for the discrepancies is the

lack of understanding about secondary aerosols formed from vehicle exhaust.

Direct motor vehicle emission of PM is predominantly from diesel vehicles (Reff et al., 2009; Zhang et al., 2009). In China diesel vehicles contributed more than 99% of primary vehicle emission of PM although they only account for 15.2% of China's on-road vehicles (MEPC, 2014). Recent studies in Beijing revealed that diesel vehicles contribute 80%–90% of PM emissions from on-road sources (Huo et al., 2011; Wu et al., 2010; Wang et al., 2010). Hence, restriction of diesel vehicles into the core urban areas has become a control measure widely adopted by municipal governments to improve air quality. Besides primary particle emission, vehicle exhaust also contributes substantially to gaseous pollutants, such as volatile organic compounds (VOCs) and nitrogen oxides (NO_x), which can form secondary organic and inorganic aerosols via photo-oxidation (Weitkamp et al., 2007; Robinson et al., 2007; Nordin et al., 2013; Liu et al., 2015a). Nordin et al. (2013) reported that secondary organic aerosols (SOA) formed from gasoline exhaust can reach as high as 500 times that of primary organic aerosols (POA). Although primary PM emission factors of diesel vehicles are typically orders of magnitude higher than gasoline vehicles, recent studies demonstrated that for diesel vehicles the SOA/POA ratios could reach about 3 based on chamber simulations (Chirico et al., 2010; Gordon et al., 2014b). Consequently, contribution of vehicle exhaust to ambient fine particles would become more complicated if considering secondary aerosol formation.

In China, a large portion of gasoline vehicles are produced in Sino-Foreign joint

ventures and due to transfer of gasoline engine technology from abroad, chamber simulation study showed that the SOA/POA ratios for China's gasoline vehicle exhaust are quite similar with those reported in the Europe or in the US (Liu et al., 2015a). However, engines equipped on China's diesel vehicles are mainly designed and produced domestically with their technology lagging behind the developed nations. According to previous studies (Yanowitz, 2000; Cheung et al., 2009; Liu et al., 2009), the emission factors of both hydrocarbon and particulate matter for diesel vehicles in China were much higher than those in the developed nations. Therefore, the SOA formation from China's diesel exhaust may be different with those in Europe and the US as well. Furthermore, most diesel vehicles in China are not equipped with emission control aftertreatment devices, which can significantly reduce both POA emission and SOA formation (Chirico et al., 2010; Gordon et al., 2014b). As previous study indicates that even for diesel vehicles SOA might dominate over POA (Gentner et al., 2012), formation of SOA from diesel vehicles in China would be an issue of wide concern.

In this study, we chose three typical types of diesel vehicles made in China, introduced the exhaust from the diesel vehicles under warm idling condition into an indoor smog chamber with a 30 m^3 reactor, and investigated the SOA formation under photo-oxidation. The main purpose of this study is to obtain a more comprehensive evaluation of diesel vehicle's contribution to carbonaceous aerosols by studying SOA formation from the primarily emitted exhaust.

2 Materials and methods

2.1 Vehicles and fuel

Table 1 lists the three diesel vehicles used for our chamber experiments. They represent three different types of diesel vehicles manufactured by three major diesel vehicle makers in China. Foton is a medium-duty passenger vehicle made by the Baic Motor Corporation LTD., Changan is a medium-duty truck made by the China Changan Automobile Group, and JAC is a heavy-duty truck made by the JAC Motors. In 2011, the diesel vehicle productions of the three companies were 490,280, 299,506 and 230,452, respectively (China Automotive Industry Yearbook, 2012), and their diesel vehicle sales were all among the top 10 in China. All the vehicles in this study had no exhaust aftertreatment devices and they were fueled with Grade 0# diesel, which complies with the Euro III diesel fuel standard.

2.2 Experimental setup

The experiments were carried out in the indoor smog chamber at Guangzhou Institute of Geochemistry, Chinese Academy of Sciences (GIG-CAS) with a ~30 m^3 Teflon reactor suspended in a temperature-controlled room. Details of setup and facilities about the chamber were described elsewhere (Wang et al., 2014a). Briefly, 135 black lamps (1.2 m long, 60 W Philips/ 10R BL, Royal Dutch Philips Electronics Ltd., the Netherlands) are used as light source, providing a NO_2 photolysis rate of 0-0.49 min^{-1}. Temperature can be set in a range from -10 to 40°C with an accuracy of ±1°C, and is measured by eight sensors inside the enclosure and the other one inside the Teflon

reactor. In this study, temperature and relative humidity (RH) for all experiment were set to 25°C and less than 5%, respectively. Prior to each experiment, the Teflon chamber was flushed with dry purified air for at least 48 hours, which represents at least 5 whole exchanges of the reactor volume. Before each experiment, the chamber was checked for hydrocarbons, ozone, NO_x, and particles inside the reactor to make sure it was clean.

Before introducing exhaust into the chamber reactor, all vehicles in the experiments were at "warm idling" mode, which means the vehicles were started and run on-road for about 30min before staying at idling condition. Diesel vehicle exhaust was introduced into the purified air filled chamber using a Dekati® ejector dilutor (DI-1000, Dekati Ltd., Finland) connected to the end of the stainless steel transfer line (0.5 inch i.d. and 15 meters in length) heated at 100°C. When the particle mass reached approximate 50 μg m^{-3}, which is comparable to the annual average value of $PM_{2.5}$ in Guangzhou (Guangzhou Environmental Protection Bureau, 2014), we stopped injecting exhaust. The injection time ranged from 5 to 20 min. The dilution ratios were estimated by measuring the CO_2 concentrations and showed in Table 2.

After introducing exhaust, nitrous acid (HONO) was bubbled into the chamber as a source of hydroxyl radical (OH). Propene was added to adjust the VOC/NO_x ratios to approximately 3:1 ppbC:ppb, which is considered as an typical ratio for urban environments (Guo et al., 2013). Propene has often been added to adjust VOC/NO_x ratio in diesel exhaust chamber experiments (Chirico et al., 2010; Presto et al., 2014;

Gordon et al., 2014b) and is not considered to be a relevant SOA precursor (Odum et al., 1996; Coker et al., 2001). 60 ppbv of deuterated butanol (butanol-d9) was also injected into the chamber as an OH tracer by using $k_{\text{butanol-d9}} = 3.4\times10^{-12}$ cm^3 $molecule^{-1}s^{-1}$ (Barmet et al., 2012; Gordon et al., 2014a). After characterizing the primary emissions in a dark condition for an hour, the exhaust was photo-oxidized for 5 h by being exposed to black lights.

2.3 Instrumentation

An array of instruments was used to monitoring trace gases and particles inside the chamber. Ozone (O_3) was measured with an ozone analyzer (EC9810, Ecotech, Australia) and NO_x were measured with a trace nitrogen oxides analyzer (EC9841, Ecotech, Australia). SO_2 was measured with a dedicated analyzer (Model 43i, Thermo Scientific, USA). VOCs were measured online with a commercial proton-transfer-reaction time-of-flight mass spectrometer (PTR-TOF-MS, Model 2000, Ionicon Analytik GmbH, Austria) (Lindinger et al., 1998; Jordan et al., 2009). Offline VOC samples were also collected using 2L stainless steel canisters each 30 min during the photo-oxidation, and measured by a Model 7100 Preconcentrator (Entech Instruments Inc., California, USA) coupled with an Agilent 5973N gas chromatography-mass selective detector/flame ionization detector (GC-MSD/FID, Agilent Technologies, USA). CO in the canister samples was analyzed using a gas chromatography (6980GC, Agilent, USA) with a flame ionization detector and a packed column (5A molecular sieve 60/80 mesh, 3 m×1/8 inch). Detailed procedures

for the offline analysis of VOCs and CO were described elsewhere (Zhang et al., 2012). Before and after introducing exhaust, air samples were collected into 3L cleaned Teflon bags to determine CO_2 concentrations with an HP 4890D gas chromatography (Yi et al., 2007).

A scanning mobility particle sizer (SMPS, Model 3080 classifier, model 3775 CPC; TSI Inc., Minnesota, USA) was used to measure particle number and volume concentrations and size distributions. The particle mass concentration was estimated assuming spherical particles and a density of 1.0 g cm^{-3} (Weitkamp et al., 2007). BC concentrations were measured with a seven-channel Aethalometer (Model AE-31, Magee Scientific, Berkeley, California). The Aethalometer data were corrected for particle loading effects using the method of Kirchstetter and Novakov (2007). A high-resolution time-of-flight aerosol mass spectrometer (HR-ToF-MS, Aerodyne Research Inc., USA) operated in alternating mode were used to measure nonrefractory submicron aerosol mass and chemical compositions (Jayne et al., 2000; DeCarlo et al., 2006). The average operating time was 1 min for the high-sensitivity V mode and 1 min for high-resolution W mode. The toolkit Squirrel 1.53G was used to analyze time series of various mass components, and Pika 1.12G was used to determine the average element ratios (http://cires1.colorado.edu/jimenez-group/ToFAMSResources/ToFSoftware/index.html). For elemental analysis, the data were analyzed based on the method described in Aiken et al. (2007, 2008). The fragmentation table from Allan et al. (2004) was used to interpret the AMS data. The contribution of gas phase CO_2 to the AMS *m/z* 44 signal was corrected by analyzing HEPA filtered air from the smog

chamber after filling the exhaust.

2.4 Operation Steps

Each experiment consisted of five steps: 1) Introducing exhaust into the chamber from t=-2h. With the injection of exhaust, concentrations of NO_x, BC and OA were climbing. Their concentrations when the injection stopped are shown in Table 2. The mixing ratio of NO_x increased from 0 to ~1 ppmv; the particle number concentration increased fast from ~2 to ~350,000 particles cm^{-3}; the total particle mass concentrations increased from ~0 to over 100 μg m^{-3}; and the VOC concentrations also slightly increased at this step. 2) Characterizing primary emissions from t =−1.5h. After completion of injection, the increase of NO_x, BC, OA and VOCs were measured against that of CO_2 and CO, and the emission factors were further calculated based on equation (1). 3) Adding HONO and propene at approximately t =−0.5h, leading to a moderate increasing of both NO and NO_2, approximately 300 ppbv for each. 4) Turning on the lights at t = 0 h to start the photo-oxidation. Substantial amounts of SOA formed at the beginning of this period. 5) Turning off the light at t=5h and further characterizing the aged diesel vehicle exhaust in the dark for about 2 hours.

2.5 Data analysis

The emission factors (EF) for various pollutants and the production factors (PF) for SOA were calculated on a fuel basis (g kg-$fuel^{-1}$):

$$EF_P \text{ or } PF_P = 10^3 \cdot [\Delta P]/(\frac{[\Delta CO_2]}{MW_{CO_2}} + \frac{[\Delta CO]}{MW_{CO}}) \cdot \frac{C_f}{MW_C} \qquad (1)$$

Where $[\Delta P]$ is the background corrected pollutant concentration in μg m^{-3}, $[\Delta CO_2]$

and [ΔCO] is the background-subtracted concentration of CO_2 and CO in the chamber in μg m^{-3}. MW_{CO2}, MW_{CO} and MW_C are the molecular weights of CO_2 (44.1 g mol^{-1}), CO (28 g mol^{-1}) and carbon (12 g mol^{-1}), respectively. C_f is the mass faction of carbon in the diesel fuel, which was adopted as 0.87 kg C kg-$fuel^{-1}$ for diesel (Chirico et al., 2010). Equation (1) assumes that all carbon in the fuel was converted to CO_2 and CO, and the contribution from VOC was negligible. This assumption was reasonable, because [ΔCO_2] and [ΔCO] after introducing exhaust were approximate 100 ppmv and 1 ppmv, respectively, while the increase of VOC was below 5ppbv. The concentrations of hydroxyl radical (OH) during the experiments were inferred from the decay of deuterated butanol measured with the PTR-MS (Atkinson and Arey, 2003). The average OH levels during our experiments were calculated to be approximate 2-5×10^6 molecules cm^{-3}, which approached to the levels in the ambient and that in the previous study by Gordon et al. (2014b).

The loss of particles and condensable organic vapors onto the reactor walls need to be corrected to accurately quantify particle concentrations in the smog chamber. In this study, the AMS and SMPS data were corrected for wall loss using the method of Gordon et al. (2014b). Briefly, particulate losses were quantified by assuming that the aerosol was internally mixed and thus, organic aerosol (OA) had the same wall-loss rates with BC. Two limiting cases were considered: ω=0, no organic vapors condense to wall-bound particles; ω=1, organic vapors remain in equilibrium with both wall-bound and suspended particles, where ω is a proportionality factor of organic vapor partition to chamber walls and suspended particles (Weitkamp et al., 2007).

For ω=0, the loss rate of OA to the chamber wall is

$$\frac{d}{dt}(OA_{wall}) = -k \times OA_{sus} \qquad (2)$$

Where OA_{wall} and OA_{sus} are the wall-bounded and the suspended OA measured at time *t*, respectively, and *k* is the wall loss rate constant of BC. The total concentration of OA at time t ($OA_{total,t}$) was calculated by:

$$OA_{total,t} = OA_{sus}(t) + \int_0^t k \cdot OA_{sus}(t)dt \qquad (3)$$

For ω=1, the total concentration of OA at time *t* ($OA_{total,t}$) was estimated as:

$$OA_{total,t} = OA_{sus}(t) \times [BC(t_0)/BC(t)] \qquad (4)$$

Where $BC(t_0)$ was the initial BC concentration measured before lights were switched on and $BC(t)$ was the BC concentration after lights were turned on for a time span *t*.

In the experiments with low BC concentrations, we corrected the wall loss effect using exponential fit to the BC data rather than the actual BC data themselves (Gordon et al., 2014b):

$$OM_{WLC} = OM_{Meas}(t)/e^{-kt} \qquad (5)$$

Where *k* is the wall loss rate constant of black carbon which obtained after lights were switched off.

Ion enhancement ratios (IER) of the selected ions from the mass spectra of AMS were calculated to evaluate the chemical evolution of POA with aging. The method described by Chirico et al. (2010) is used in this study, and the IER is defined as:

$$\text{IER} = [Ion(t)/Ion(t_0)]/[BC(t)/BC(t_0)] \qquad (6)$$

Where $Ion(t)$ and $Ion(t_0)$ are the ion signals at time $\boldsymbol{t}$ and at the time when the lights were just turned on ($\boldsymbol{t_0}$), respectively.

3 Results and discussions

3.1 Emission factors of carbonaceous aerosols (BC and POA)

The emission factors of POA and BC are shown in Figure 1. The EF_{BC} were 0.15-0.51 g kg-fuel^{-1} in this study, comparable with those of 0.466-0.763 g kg-fuel^{-1} reported by Chirico et al. (2010) and ~0.260 g kg-fuel^{-1} by Gordon et al. (2014b) at idling condition. Nevertheless, the EF_{POA} (0.18-0.91 g kg-fuel^{-1}) were higher than those from previous studies. For instance, the highest emission factors for POA reported by Chirico et al. (2010) were only 0.147 g kg-fuel^{-1}. As the diesel fuel used in this study is at Euro III standard, in which the sulfur content is approximately 350 ppm (Zhang et al., 2010; Yue et al., 2015), which is much higher than that employed in previous studies. Moreover, the fuel sulfur content can affect the particle emission for diesel vehicle (Rönkkö et al., 2007). Therefore, the relatively backward diesel engine technology and low quality of diesel fuel would probably be the reasons for higher EFs of POA for China's diesel vehicles in this study.

3.2 SOA formation from diesel vehicle exhaust

Figure 2 shows the typical temporal evolution of gas and particle phase species during a smog chamber experiment (Experiment 8). As showed in Figure 2(c), wall-loss corrected OA started to climb with the formation of SOA after turning on the lights.

After 5 h photo-oxidation, the wall loss corrected OA in Experiment 8 increased from 64 μg m^{-3} to 112 μg m^{-3} for ω=0 case and to 166 μg m^{-3} for ω=1 case. However, while the median diameters were increasing with aging (Figure 3(a)), there was no sign of increasing particle numbers, indicating few new particles were formed. Moreover, as shown in Figure 3(b), after about half an hour photo-oxidation (t=0.4), the number of small particles dropped fast, whereas the number concentration of larger particles almost did not change, and the peak diameter slightly increased. It suggested particle growth by coating of the newly formed SOA on existing particles, consistent with the results of Weitkamp et al. (2007).

PF_{SOA} (0.50-1.8 g kg-$fuel^{-1}$) from this study were much higher than those from previous studies, as the highest PF of SOA reported by Chirico et al. (2010) for a medium-duty diesel vehicle (MDDV) at idling condition in Switzerland was merely 0.461 g kg-$fuel^{-1}$. The SOA/POA ratios for all the experiments ranged from 0.6 to 2.4 in this study, lower than that of ~3 for a MDDV at idling condition as reported by Chirico et al. (2010) and the value of approximately 10 for a heavy-duty diesel vehicle (HDDV) at creep condition in the US as reported by Gordon et al. (2014b). As shown in Table 2, the O:C ratios were higher than previous study (Chirico et al., 2010), while the aerosol volatility and O:C are generally inversely correlated (Lanz et al., 2007; Jimenez et al., 2009; Ulbrich et al., 2009), this demonstrated that less organics was partitioned to gas phase during the dilution(Donahue et al., 2006). Moreover, the reaction rate in gas phase is faster than that in particle phase (Esteve et al., 2006; Bedjanian et al., 2010). Therefore, the lower volatility of emitted organics

could cause less SOA formation.

Whether gasoline or diesel dominates the vehicular OA is still controversial (Bahreini et al., 2012; Gentner et al., 2012; Jathar et al., 2014). As reported by previous study , the highest EF_{POA} and PF_{SOA} for gasoline vehicle exhaust in China were 0.0004 g kg-fuel^{-1} and 0.044 g kg-fuel^{-1}, respectively (Liu et al., 2015a), which are 1-3 orders of magnitude lower than those for diesel vehicle exhaust according to this study. For this reason, diesel vehicle exhaust would still account for a larger portion of traffic-related primary and secondary OA, despite higher faction of gasoline vehicles (83.5%) against that of diesel vehicles (15.2%) in China (MEPC, 2014). As reported by Ou et al. (2010), the fuel consumption of diesel and gasoline for road transportation is 38.53 and 52.20 million tons in 2007, so with the POA emission factors and SOA production factors available in this study and in a previous study for gasoline exhaust (Liu et al., 2015a), the diesel derived OA would dominate overwhelmingly over the gasoline derived OA in the vehicular OA.

3.3 SOA yield from precursor VOCs

Aromatic hydrocarbons were considered as very important anthropogenic SOA precursors (Odum et al., 1997). For gasoline vehicle exhaust, aromatics account for 51-90% of formed SOA (Nordin et al., 2013; Liu et al., 2015a). SOA production from aromatics, including benzene, toluene, C_2-benzene, C_2-benzene, C_4-benzene, was estimated by the following formula:

$$SOA_{predicted} = \sum_i \Delta X_i \times Y_i \qquad (6)$$

Where $SOA_{predicted}$ (μg m^{-3}) is the predicted SOA concentration from precursor *i*; ΔX_i (μg m^{-3}) is the mass of the reacted precursor *i* which was inferred from PRT-ToF-MS data; and Y_i (%) is the SOA yield of precursor *i*. In this study, SOA yields for benzene, toluene, and m-xylene were estimated using the two-product model curves taken from Ng et al. (2007) and those for C_3-benzene and C_4-benzene were taken from Odum et al. (1997).

As presented in Table 3, the predicted SOA concentrations from traditional aromatic precursors accounted for less than 3% of the observed SOA production. Similarly, Weitkamp et al. (2007) reported that SOA formed from 58 known precursors, including aromatics, alkanes and alkenes, just explained less than 8% of the new particle mass in diesel exhaust simulation. It demonstrated that traditional VOC precursors could not explain the amount of diesel SOA formation. One possible reason is that the yields of aromatic hydrocarbons in complex mixture condition might be higher than those in single precursor condition (Song et al, 2007a), thus the SOA mass was probably underestimated. However, even if we took a higher aromatics yield, such as the effective SOA yield of ~30% reported by Gordon et al. (2014b), aromatics only accounted for less than 10% of total SOA, the discrepancies between predicted and measured SOA were still huge. The unexplained part is probably from the photo-oxidation of the intermediate volatile organic compounds (IVOCs)

(Weitkamp et al., 2007; Robinson et al., 2007), such as C_{13}-C_{20} *n*-alkanes (Miracolo et al., 2010).

It worth noting that there would be other oxygenated species, like glyoxal and methyl glyoxal, were considered as potential SOA precursors (Volkamer et al., 2006; Carlton et al., 2007; Fu et al., 2008; Kamens et al., 2011). Glyoxal and methyl glyoxal can be primarily emitted from vehicles (Zhang et al., 2016), or secondarily formed by the photo-oxidation of VOCs (Carlton et al., 2007; Healy et al., 2008; Volkamer et al., 2009). The PTR-ToF-MS measured ion *m/z* 59 represents acetone and glyoxal, and ion *m/z* 73 represents methyl glyoxal (Healy et al., 2008; Kahnt et al., 2011). As acetone is mainly biogenic (Jacob et al., 2002), or produced via oxidation of C_3-C_5 isoalkanes (Fu et al., 2008), which were only 1-2 ppbv during the experiments, therefore, the signal of *m/z* 59 is mainly glyoxal. The evolution of *m/z* 59 and *m/z* 73 was shown in Figure 4. When we introduced diesel vehicle exhaust, the mixing ratios of *m/z* 59 and *m/z* 73 increased from ~0 to 11 and to 2.5 ppbv, respectively; after 5 hours photo-oxidation, the mixing ratios of *m/z* 59 and *m/z* 73 further increased to 71 and 6.0 ppbv, indicating secondary formation of glyoxal and methyl glyoxal during photo-oxidation. Therefore, the primary and secondary glyoxal and methyl glyoxal could also partly explain the SOA formation from diesel vehicle exhaust.

3.4 Chemical evolution of OA

Figure 5 showed the average AMS mass spectra for the total OA measured in the beginning and at the end of a typical simulation (Experiment 8). According to the

method described by Chirico et al. (2010), high resolution mass spectra was divided into 4 organic fragment classes, namely CH, CHO (including fragments only with C and O), CHN and CHON.

Very similar to those in previous studies (Weitkamp et al., 2007; Chirico et al., 2010; Presto et al., 2014), POA spectra in the beginning were dominated by the $C_nH_{2n+1}^+$ organic fragment ion group (*m/z* 29, 43, 57, 71,…) characteristic of alkanes (Figure 5(a)). They also had a prominent $C_nH_{2n-1}^+$ sequence (*m/z* 27, 41, 55, 69,…) that is associated with cycloalkanes and alkenes (Canagaratna et al., 2004). The POA from all the experiment show that the largest signal contribution is from *m/z* 43 (47% of which is $C_3H_7^+$, and 52% of which is $C_2H_3O^+$), followed by *m/z* 41 (97 % of which is $C_3H_5^+$). A certain amount of signals for PAHs, such as *m/z* 128 for naphthalene, 152 for acenaphthylene, 178 for phenanthrene or anthracene and 202 for fluoranthene or pyrene, were also observed, and the fractions of these fragments in total OA signal were 0.5%, 0.3%, 0.2% and 0.1%, respectively. Overall, In the beginning CH class took the largest fraction of approximate 67.6% in total OA, followed by the CHO class (29.2%), while the fractions of CHN (1.8%) and CHON (1.4%) class were much lower. Compared with the distribution pattern (75.2% for CH and 22.8% for CHO) reported by Chirico et al. (2010), POA spectra in this study had a lower CH class but higher CHO class, suggesting more oxidized components in the initially emitted exhaust.

The aged OA mass spectrum shown in Figure 5(b) is averaged over the last one hour

of the experiment. After 5-hour aging, the contribution to total organic mass by fragments *m/z* 44, representing oxidized organics with ~98% of which consisted of CO_2^+ and $C_2H_4O^+$, increased from 5.6% to 10.6%. Meanwhile, the signal of *m/z* 57, which generally associated with primary emissions (Weitkamp et al., 2007; Sage et al., 2008), dropped form 3.7% to 2.2%. Moreover, the fraction of $C_3H_7^+$ in *m/z* 43 decreased drastically from 47% to 17%, whereas the fraction of $C_2H_3O^+$ in *m/z* 43 increased from 55% to 81%. The relative contribution of the ion classes also changed significantly after 5 hours photo-oxidation compared to those of POA. The fraction of CH class fell from 67.6% to 48.3%, whereas that of the CHO class grew from 29.2% to 47.6%, indicating a more oxidized chemical property. The CHN and CHON classes contributed 2.3% and 1.7%, respectively; they were also minor components although their factions were becoming higher.

Figure 6 presents typical temporal evolutions of the H/C and O/C atomic ratios as well as the OM/OC ratio measured by the AMS (Experiment 8). With photo-oxidation, the average ratios for O/C and OM/OC slightly increased from 0.26 to 0.47 and from 1.48 to 1.76, respectively; while that for H/C ratio decreased from 1.50 to 1.43. The increase of O/C and OM/OC ratios and decrease of H/C ratios after photo-oxidation were found during all the experiments (Table 2), further confirming the increased oxidation state of OA during aging. It should be pointed out that the increase of oxidation state is due to not only the formation of SOA, but also further oxidation or degradation of POA. For example, as shown in Figure 7, the IERs of polycyclic aromatic hydrocarbons (PAHs) signals such as $C_{10}H_8^+$, $C_{12}H_8^+$, $C_{14}H_{10}^+$, $C_{16}H_{10}^+$

(Bruns et al., 2015; Elster et al., 2016), which represent naphthalene, acenaphthylene, phenanthrene or anthracene, fluoranthene or pyrene, respectively, decreased substantially after 5-hour aging. It indicates that PAHs, probably along with other POA species, were oxidized through heterogeneous reaction, or vaporized to gas phase, oxidized and then condensed back onto particles (Donahue et al., 2006; Robinson et al., 2007).

The f_{43} versus f_{44} triangle plot for OA in our experiments is presented in Figure 8(a). Compared with POA, SOA had higher f_{44} and lower f_{43} values. According to Ng et al. (2010), ambient low-volatility oxygenated OA (LV-OOA) and SV-OOA factors fall in the upper and lower portions of the triangle, respectively. Similar with that reported by Presto et al. (2014) for diesel SOA, the plots of SOA were within the range of SV-OOA. Figure 8(b) translates the AMS data into van Krevelen space. The van Krevelen slopes for this study ranged from -0.47 to -0.68, which were similar to that reported by Presto et al. (2014) for diesel exhaust experiments, and also in the range of slopes for ambient OOA factors observed by Ng et al. (2011). It indicates that the SOA chemistry observed in present smog chamber experiments is atmospherically relevant (Presto et al., 2014). According to Heald et al. (2010) and Ng et al. (2011), slopes of -1 and 0 in the Van Krevelen diagram represent chemical reaction for addition of carboxylic acid and alcohol/peroxide, respectively. Therefore, the van Krevelen slopes in this study suggest that SOA formed was a combination of carboxylic acids and alcohols/peroxides.

4 Conclusions

In this paper, chamber simulations were conducted to investigate SOA formation from diluted exhaust of three types of diesel vehicles widely used in China. EF_{POA} and PF_{SOA} in this work were 0.19 and 0.61 g kg-fuel^{-1} for JAC, 0.18-0.34 and 0.56-0.76 g kg-fuel^{-1} for Foton, 0.72-0.91 and 0.50-1.8 g kg-fuel^{-1} for Changan, respectively, which were all higher than those reported in previous studies in Europe and in the US. These EF_{POA} and PF_{SOA} values were also 2-3 and 1 orders of magnitude higher than those of gasoline vehicle exhaust. Therefore, although diesel vehicle population is much less than that of gasoline in China, it still plays a vital role in the contribution of primary and secondary OA. Moreover, POA in our study had much higher O/C ratio and less volatility, this could partly explain lower ratios of SOA/POA in this study. It should be noted that all the experiments for SOA formation from both gasoline and diesel vehicles in China were conducted under idling condition. The emission of POA as well as formation SOA under different operating modes, especially on-road conditions, deserves further investigation.

According to our study, less than 3% of diesel SOA production can be explained by aromatics, consistent with previous diesel exhaust studies. It demonstrated that there existed substantial unknown precursors. Photo-oxidation of high molecular weight hydrocarbons (PAHs), as well as heterogeneous reaction of oxygenated species like glyoxal and methyl glyoxal, might contribute to the SOA formation from diesel vehicle exhaust. SOA from diesel vehicles belongs to SV-OOA based on AMS data.

445 The van Krevelen slopes in our experiments were between -0.47 and -0.68, suggesting
446 that SOA formed is a combination of carboxylic acids and alcohols/peroxides.

447 **Acknowledgments**

448 This study was supported by the Strategic Priority Research Program of the Chinese
449 Academy of Sciences (XDB05010200), the National Natural Science Foundation of
450 China (41025012/41571130031).

451 **References**

452 Aiken, A. C., DeCarlo, P. F., and Jimenez, J. L.: Elemental analysis of organic species
453 with electron ionization high-resolution mass spectrometry, Anal. Chem., 79,
454 8350-8358, doi:10.1021/ac071150w, 2007.
455 Aiken, A. C., DeCarlo, P. F., Kroll, J. H., Worsnop, D. R., Huffman, J. A., Docherty, K.
456 S., Ulbrich, I. M., Mohr, C., Kimmel, J. R., Sueper, D., Sun, Y., Zhang, Q.,
457 Trimborn, A., Northway, M., Ziemann, P. J., Canagaratna, M. R., Onasch, T. B.,
458 Alfarra, M. R., Prevot, A. S. H., Dommen, J., Duplissy, J., Metzger, A.,
459 Baltensperger, U., and Jimenez, J. L.: O/C and OM/OC ratios of primary, secondary,
460 and ambient organic aerosols with high-resolution time-of-flight aerosol mass
461 spectrometry, Environ. Sci. Technol., 42, 4478-4485, doi:10.1021/es703009q, 2008.
462 Allan, J. D., Delia, A. E., Coe, H., Bower, K. N., Alfarra, M. R., Jimenez, J. L.,
463 Middlebrook, A. M., Drewnick, F., Onasch, T. B., Canagaratna, M. R., Jayne, J. T.,
464 and Worsnop, D. R.: A generalised method for the extraction of chemically resolved
465 mass spectra from aerodyne aerosol mass spectrometer data, Int. J. Mass Spectrom.

Ion Processes, 35, 909-922, doi:10.1016/j.jaerosci.2004.02.007, 2004.

Atkinson, R., and Arey, J.: Atmospheric degradation of volatile organic compounds, Chem. Rev., 103, 4605-4638, doi:10.1021/cr0206420, 2003.

Bahreini, R., Middlebrook, A. M., de Gouw, J. A., Warneke, C., Trainer, M., Brock, C. A., Stark, H., Brown, S. S., Dube, W. P., Gilman, J. B., Hall, K., Holloway, J. S., Kuster, W. C., Perring, A. E., Prevot, A. S. H., Schwarz, J. P., Spackman, J. R., Szidat, S., Wagner, N. L., Weber, R. J., Zotter, P., and Parrish, D. D.: Gasoline emissions dominate over diesel in formation of secondary organic aerosol mass, Geophys. Res. Lett., 39, doi:10.1029/2011GL050718, 2012.

Barmet, P., Dommen, J., DeCarlo, P. F., Tritscher, T., Praplan, A. P., Platt, S. M., Prevot, A. S. H., Donahue, N. M., and Baltensperger, U.: OH clock determination by proton transfer reaction mass spectrometry at an environmental chamber, Atmos. Meas. Tech., 5, 647-656, doi:10.5194/amt-5-647-2012, 2012.

Bedjanian, Y., Nguyen, M. L., and Le Bras, G.: Kinetics of the reactions of soot surface-bound polycyclic aromatic hydrocarbons with the OH radicals, Atmos. Environ., 44, 1754-1760, doi:10.1016/j.atmosenv.2010.02.007, 2010.

Brook, R. D., Rajagopalan, S., Pope, C. A., 3rd, Brook, J. R., Bhatnagar, A., Diez-Roux, A. V., Holguin, F., Hong, Y., Luepker, R. V., Mittleman, M. A., Peters, A., Siscovick, D., Smith, S. C., Jr., Whitsel, L., Kaufman, J. D., and on behalf of the American Heart Association Council On Epidemiology and Prevention, Council on the Kidney in Cardiovascular Disease, Council on Nutrition, Physical Activity and Metabolism: Particulate matter air pollution and cardiovascular disease: An

488 update to the scientific statement from the American Heart Association, Circulation,
489 121, 2331-2378, doi:10.1161/CIR.0b013e3181dbece1, 2010.
490 Bruns, E. A., Krapf, M., Orasche, J., Huang, Y., Zimmermann, R., Drinovec, L.,
491 Močnik, G., El-Haddad, I., Slowik, J. G., Dommen, J., Baltensperger, U., and
492 Prévôt, A. S. H.: Characterization of primary and secondary wood combustion
493 products generated under different burner loads, Atmos. Chem. Phys., 15,
494 2825-2841, doi:10.5194/acp-15-2825-2015, 2015.
495 Canagaratna, M. R., Jayne, J. T., Ghertner, D. A., Herndon, S., Shi, Q., Jimenez, J. L.,
496 Silva, P. J., Williams, P., Lanni, T., Drewnick, F., Demerjian, K. L., Kolb, C. E., and
497 Worsnop, D. R.: Chase studies of particulate emissions from in-use New York City
498 vehicles, Aerosol Sci. Technol., 38, 555-573, doi:10.1080/02786820490465504,
499 2004.
500 Carlton, A. G., Turpin, B. J., Altieri, K. E., Seitzinger, S., Reff, A., Lim, H.-J., and
501 Ervens, B.: Atmospheric oxalic acid and SOA production from glyoxal: Results of
502 aqueous photooxidation experiments, Atmos. Environ., 41, 7588-7602,
503 doi:10.1016/j.atmosenv.2007.05.035, 2007.
504 Chen, Y., Zheng, M., Edgerton, E. S., Ke, L., Sheng, G., and Fu, J.: $PM_{2.5}$ source
505 apportionment in the southeastern U.S.: Spatial and seasonal variations during
506 2001–2005, J. Geophys. Res., 117, D08304, doi:10.1029/2011JD016572, 2012.
507 Cheung, K. L., Polidori, A., Ntziachristos, L., Tzamkiozis, T., Samaras, Z., Cassee, F.
508 R., Gerlofs, M., and Sioutas, C.: Chemical characteristics and oxidative potential of
509 particulate matter emissions from gasoline, diesel, and biodiesel cars, Environ. Sci.

510 Technol., 43, 6334-6340, doi:10.1021/es900819t, 2009.
511 China Association of Automobile Manufactures, China Automotive Industry Yearbook
512 2011, 2012.
513 Chirico, R., DeCarlo, P. F., Heringa, M. F., Tritscher, T., Richter, R., Prevot, A. S. H.,
514 Dommen, J., Weingartner, E., Wehrle, G., Gysel, M., Laborde, M., and
515 Baltensperger, U.: Impact of aftertreatment devices on primary emissions and
516 secondary organic aerosol formation potential from in-use diesel vehicles: results
517 from smog chamber experiments, Atmos. Chem. Phys., 10, 11545-11563,
518 doi:10.5194/acp-10-11545-2010, 2010.
519 Cocker, D. R., Mader, B. T., Kalberer, M., Flagan, R. C., and Seinfeld, J. H.: The
520 effect of water on gas-particle partitioning of secondary organic aerosol: II.
521 m-xylene and 1,3,5-trimethylbenzene photooxidation systems, Atmos. Environ., 35,
522 6073-6085, doi:10.1016/s1352-2310(01)00405-8, 2001.
523 Cui, H., Chen, W., Dai, W., Liu, H., Wang, X., and He, K.: Source apportionment of
524 $PM_{2.5}$ in Guangzhou combining observation data analysis and chemical transport
525 model simulation, Atmos. Environ., 116, 262-271,
526 doi:10.1016/j.atmosenv.2015.06.054, 2015.
527 DeCarlo, P. F., Kimmel, J. R., Trimborn, A., Northway, M. J., Jayne, J. T., Aiken, A.
528 C., Gonin, M., Fuhrer, K., Horvath, T., Docherty, K. S., Worsnop, D. R., and
529 Jimenez, J. L.: Field-deployable, high-resolution, time-of-flight aerosol mass
530 spectrometer, Anal. Chem., 78, 8281-8289, doi:10.1021/ac061249n, 2006.
531 Donahue, N. M., Robinson, A. L., Stanier, C. O., and Pandis, S. N.: Coupled

partitioning, dilution, and chemical aging of semivolatile organics, Environ. Sci. Technol., 40, 2635-2643, doi:10.1021/es052297c, 2006.

Elser, M., Huang, R. J., Wolf, R., Slowik, J. G., Wang, Q., Canonaco, F., Li, G., Bozzetti, C., Daellenbach, K. R., Huang, Y., Zhang, R., Li, Z., Cao, J., Baltensperger, U., El-Haddad, I., and Prévôt, A. S. H.: New insights into PM2.5 chemical composition and sources in two major cities in China during extreme haze events using aerosol mass spectrometry, Atmos. Chem. Phys., 16, 3207-3225, doi:10.5194/acp-16-3207-2016, 2016.

Esteve, W., Budzinski, H., and Villenave, E.: Relative rate constants for the heterogeneous reactions of NO_2 and OH radicals with polycyclic aromatic hydrocarbons adsorbed on carbonaceous particles. Part 2: PAHs adsorbed on diesel particulate exhaust SRM 1650a, Atmos. Environ., 40, 201-211, doi:10.1016/j.atmosenv.2004.05.059, 2006.

Fu, T.-M., Jacob, D. J., Wittrock, F., Burrows, J. P., Vrekoussis, M., and Henze, D. K.: Global budgets of atmospheric glyoxal and methylglyoxal, and implications for formation of secondary organic aerosols, J. Geophys. Res., 113, D15303, doi:10.1029/2007JD009505, 2008.

Gentner, D. R., Isaacman, G., Worton, D. R., Chan, A. W. H., Dallmann, T. R., Davis, L., Liu, S., Day, D. A., Russell, L. M., Wilson, K. R., Weber, R., Guha, A., Harley, R. A., and Goldstein, A. H.: Elucidating secondary organic aerosol from diesel and gasoline vehicles through detailed characterization of organic carbon emissions, Proc. Natl. Acad. Sci. USA, 109, 18318-18323, doi:10.1073/pnas.1212272109,

554 2012.
555 Gordon, T. D., Presto, A. A., May, A. A., Nguyen, N. T., Lipsky, E. M., Donahue, N.
556 M., Gutierrez, A., Zhang, M., Maddox, C., Rieger, P., Chattopadhyay, S.,
557 Maldonado, H., Maricq, M. M., and Robinson, A. L.: Secondary organic aerosol
558 formation exceeds primary particulate matter emissions for light-duty gasoline
559 vehicles, Atmos. Chem. Phys., 14, 4661-4678, doi:10.5194/acp-14-4661-2014,
560 2014a.
561 Gordon, T. D., Presto, A. A., Nguyen, N. T., Robertson, W. H., Na, K., Sahay, K. N.,
562 Zhang, M., Maddox, C., Rieger, P., Chattopadhyay, S., Maldonado, H., Maricq, M.
563 M., and Robinson, A. L.: Secondary organic aerosol production from diesel vehicle
564 exhaust: impact of aftertreatment, fuel chemistry and driving cycle, Atmos. Chem.
565 Phys., 14, 4643-4659, doi:10.5194/acp-14-4643-2014, 2014b.
566 Guangzhou Environmental Protection Bureau, Yearly report of environmental quality
567 in Guangzhou (in Chinese), 2014.
568 Guo, H., Ling, Z. H., Cheung, K., Jiang, F., Wang, D. W., Simpson, I. J., Barletta, B.,
569 Meinardi, S., Wang, T. J., Wang, X. M., Saunders, S. M., and Blake, D. R.:
570 Characterization of photochemical pollution at different elevations in mountainous
571 areas in Hong Kong, Atmos. Chem. Phys., 13, 3881-3898,
572 doi:10.5194/acp-13-3881-2013, 2013.
573 Guo, S., Hu, M., Zamora, M. L., Peng, J., Shang, D., Zheng, J., Du, Z., Wu, Z., Shao,
574 M., Zeng, L., Molina, M. J., and Zhang, R.: Elucidating severe urban haze
575 formation in China, Proc. Natl. Acad. Sci. USA, 111, 17373-17378,

576 doi:10.1073/pnas.1419604111, 2014.
577 Heald, C. L., Kroll, J. H., Jimenez, J. L., Docherty, K. S., DeCarlo, P. F., Aiken, A. C.,
578 Chen, Q., Martin, S. T., Farmer, D. K., and Artaxo, P.: A simplified description of
579 the evolution of organic aerosol composition in the atmosphere, Geophys. Res.
580 Lett., 37, L08803, doi:10.1029/2010GL042737, 2010.
581 Healy, R. M., Wenger, J. C., Metzger, A., Duplissy, J., Kalberer, M., and Dommen, J.:
582 Gas/particle partitioning of carbonyls in the photooxidation of isoprene and
583 1,3,5-trimethylbenzene, Atmos. Chem. Phys., 8, 3215-3230, 2008.
584 Huang, R. J., Zhang, Y., Bozzetti, C., Ho, K. F., Cao, J. J., Han, Y., Daellenbach, K. R.,
585 Slowik, J. G., Platt, S. M., Canonaco, F., Zotter, P., Wolf, R., Pieber, S. M., Bruns,
586 E. A., Crippa, M., Ciarelli, G., Piazzalunga, A., Schwikowski, M., Abbaszade, G.,
587 Schnelle-Kreis, J., Zimmermann, R., An, Z., Szidat, S., Baltensperger, U., El
588 Haddad, I., and Prevot, A. S.: High secondary aerosol contribution to particulate
589 pollution during haze events in China, Nature, 514, 218-222,
590 doi:10.1038/nature13774, 2014.
591 Jacob, D. J., Field, B. D., Jin, E. M., Bey, I., Li, Q., Logan, J. A., Yantosca, R. M., and
592 Singh, H. B.: Atmospheric budget of acetone, J. Geophys. Res., 107,
593 doi:10.1029/2001JD000694, 2002.
594 Jathar, S. H., Gordon, T. D., Hennigan, C. J., Pye, H. O., Pouliot, G., Adams, P. J.,
595 Donahue, N. M., and Robinson, A. L.: Unspeciated organic emissions from
596 combustion sources and their influence on the secondary organic aerosol budget in
597 the United States, Proc. Natl. Acad. Sci. USA, 111, 10473-10478,

598 doi:10.1073/pnas.1323740111, 2014.
599 Jayne, J. T., Leard, D. C., Zhang, X. F., Davidovits, P., Smith, K. A., Kolb, C. E., and
600 Worsnop, D. R.: Development of an aerosol mass spectrometer for size and
601 composition analysis of submicron particles, Aerosol Sci. Technol., 33, 49-70,
602 doi:10.1080/027868200410840, 2000.
603 Jimenez, J. L., Canagaratna, M. R., Donahue, N. M., Prevot, A. S., Zhang, Q., Kroll, J.
604 H., DeCarlo, P. F., Allan, J. D., Coe, H., Ng, N. L., Aiken, A. C., Docherty, K. S.,
605 Ulbrich, I. M., Grieshop, A. P., Robinson, A. L., Duplissy, J., Smith, J. D., Wilson,
606 K. R., Lanz, V. A., Hueglin, C., Sun, Y. L., Tian, J., Laaksonen, A., Raatikainen, T.,
607 Rautiainen, J., Vaattovaara, P., Ehn, M., Kulmala, M., Tomlinson, J. M., Collins, D.
608 R., Cubison, M. J., Dunlea, E. J., Huffman, J. A., Onasch, T. B., Alfarra, M. R.,
609 Williams, P. I., Bower, K., Kondo, Y., Schneider, J., Drewnick, F., Borrmann, S.,
610 Weimer, S., Demerjian, K., Salcedo, D., Cottrell, L., Griffin, R., Takami, A.,
611 Miyoshi, T., Hatakeyama, S., Shimono, A., Sun, J. Y., Zhang, Y. M., Dzepina, K.,
612 Kimmel, J. R., Sueper, D., Jayne, J. T., Herndon, S. C., Trimborn, A. M., Williams,
613 L. R., Wood, E. C., Middlebrook, A. M., Kolb, C. E., Baltensperger, U., and
614 Worsnop, D. R.: Evolution of organic aerosols in the atmosphere, Science, 326,
615 1525-1529, doi:10.1126/science.1180353, 2009.
616 Jordan, A., Haidacher, S., Hanel, G., Hartungen, E., Märk, L., Seehauser, H.,
617 Schottkowsky, R., Sulzer, P., and Märk, T. D.: A high resolution and high sensitivity
618 proton-transfer-reaction time-of-flight mass spectrometer (PTR-TOF-MS), Int. J.
619 Mass spectrom., 286, 122-128, doi:10.1016/j.ijms.2009.07.005, 2009.

620 Kahnt, A., Iinuma, Y., Böge, O., Mutzel, A., and Herrmann, H.: Denuder sampling
621 techniques for the determination of gas-phase carbonyl compounds: A comparison
622 and characterisation of in situ and ex situ derivatisation methods, J. Chromatogr. B,
623 879, 1402-1411, doi:10.1016/j.jchromb.2011.02.028, 2011.
624 Kamens, R. M., Zhang, H., Chen, E. H., Zhou, Y., Parikh, H. M., Wilson, R. L.,
625 Galloway, K. E., and Rosen, E. P.: Secondary organic aerosol formation from
626 toluene in an atmospheric hydrocarbon mixture: Water and particle seed effects,
627 Atmos. Environ., 45, 2324-2334, doi:10.1016/j.atmosenv.2010.11.007, 2011.
628 Kirchstetter, T. W., and Novakov, T.: Controlled generation of black carbon particles
629 from a diffusion flame and applications in evaluating black carbon measurement
630 methods, Atmos. Environ., 41, 1874-1888, doi:10.1016/j.atmosenv.2006.10.067,
631 2007.
632 Lanz, V. A., Alfarra, M. R., Baltensperger, U., Buchmann, B., Hueglin, C., and Prévôt,
633 A. S. H.: Source apportionment of submicron organic aerosols at an urban site by
634 factor analytical modelling of aerosol mass spectra, Atmos. Chem. Phys., 7,
635 1503-1522, doi:10.5194/acp-7-1503-2007, 2007.
636 Lelieveld, J., Evans, J. S., Fnais, M., Giannadaki, D., and Pozzer, A.: The contribution
637 of outdoor air pollution sources to premature mortality on a global scale, Nature,
638 525, 367-371, doi:10.1038/nature15371, 2015.
639 Lindinger, W., Hansel, A., and Jordan, A.: On-line monitoring of volatile organic
640 compounds at pptv levels by means of proton-transfer-reaction mass spectrometry
641 (PTR-MS) medical applications, food control and environmental research, Int. J.

642 Mass Spectrom. Ion Processes, 173, 191-241, doi:10.1016/S0168-1176(97)00281-4,
643 1998.
644 Liu, H., He, K., Lents, J. M., Wang, Q., and Tolvett, S.: Characteristics of diesel truck
645 emission in China based on portable emissions measurement systems, Environ. Sci.
646 Technol., 43, 9507-9511, doi:10.1021/es902044x, 2009.
647 Liu, T., Wang, X., Deng, W., Hu, Q., Ding, X., Zhang, Y., He, Q., Zhang, Z., Lü, S.,
648 Bi, X., Chen, J., and Yu, J.: Secondary organic aerosol formation from
649 photochemical aging of light-duty gasoline vehicle exhausts in a smog chamber,
650 Atmos. Chem. Phys., 15, 9049-9062, doi:10.5194/acp-15-9049-2015, 2015a.
651 Liu, Z., Guan, D., Wei, W., Davis, S. J., Ciais, P., Bai, J., Peng, S., Zhang, Q.,
652 Hubacek, K., Marland, G., Andres, R. J., Crawford-Brown, D., Lin, J., Zhao, H.,
653 Hong, C., Boden, T. A., Feng, K., Peters, G. P., Xi, F., Liu, J., Li, Y., Zhao, Y., Zeng,
654 N., and He, K.: Reduced carbon emission estimates from fossil fuel combustion and
655 cement production in China, Nature, 524, 335-338, doi:10.1038/nature14677,
656 2015b.
657 Ministry of Environmental Protection of China (MEPC). China Vehicle Emission
658 Control Annual Report 2014. 2015.
659 Miracolo, M. A., Presto, A. A., Lambe, A. T., Hennigan, C. J., Donahue, N. M., Kroll,
660 J. H., Worsnop, D. R., and Robinson, A. L.: Photo-oxidation of low-volatility
661 organics found in motor vehicle emissions: Production and chemical evolution of
662 organic aerosol mass, Environ. Sci. Technol., 44, 1638-1643,
663 doi:10.1021/es902635c, 2010.

664 Ng, N. L., Kroll, J. H., Chan, A. W. H., Chhabra, P. S., Flagan, R. C., and Seinfeld, J.
665 H.: Secondary organic aerosol formation from m-xylene, toluene, and benzene,
666 Atmos. Chem. Phys., 7, 3909-3922, doi:10.5194/acp-7-3909-2007, 2007.
667 Ng, N. L., Canagaratna, M. R., Zhang, Q., Jimenez, J. L., Tian, J., Ulbrich, I. M.,
668 Kroll, J. H., Docherty, K. S., Chhabra, P. S., Bahreini, R., Murphy, S. M., Seinfeld,
669 J. H., Hildebrandt, L., Donahue, N. M., DeCarlo, P. F., Lanz, V. A., Prévôt, A. S. H.,
670 Dinar, E., Rudich, Y., and Worsnop, D. R.: Organic aerosol components observed in
671 Northern hemispheric datasets from aerosol mass spectrometry, Atmos. Chem.
672 Phys., 10, 4625-4641, doi:10.5194/acp-10-4625-2010, 2010.
673 Ng, N. L., Canagaratna, M. R., Jimenez, J. L., Chhabra, P. S., Seinfeld, J. H., and
674 Worsnop, D. R.: Changes in organic aerosol composition with aging inferred from
675 aerosol mass spectra, Atmos. Chem. Phys., 11, 6465-6474,
676 doi:10.5194/acp-11-6465-2011, 2011.
677 Nordin, E. Z., Eriksson, A. C., Roldin, P., Nilsson, P. T., Carlsson, J. E., Kajos, M. K.,
678 Hellén, H., Wittbom, C., Rissler, J., Löndahl, J., Swietlicki, E., Svenningsson, B.,
679 Bohgard, M., Kulmala, M., Hallquist, M., and Pagels, J. H.: Secondary organic
680 aerosol formation from idling gasoline passenger vehicle emissions investigated in
681 a smog chamber, Atmos. Chem. Phys., 13, 6101-6116,
682 doi:10.5194/acp-13-6101-2013, 2013.
683 Odum, J. R., Hoffmann, T., Bowman, F., Collins, D., Flagan, R. C., and Seinfeld, J. H.:
684 Gas/particle partitioning and secondary organic aerosol yields, Environ. Sci.
685 Technol., 30, 2580-2585, doi:10.1021/es950943+, 1996.

686 Odum, J. R., Jungkamp, T. P. W., Griffin, R. J., Flagan, R. C., and Seinfeld, J. H.: The
687 atmospheric aerosol-forming potential of whole gasoline vapor, Science, 276,
688 96-99, doi:10.1126/science.276.5309.96, 1997.
689 Ou, X., Zhang, X., and Chang, S.: Scenario analysis on alternative fuel/vehicle for
690 China's future road transport: Life-cycle energy demand and GHG emissions,
691 Energy Policy, 38, 3943-3956, doi:10.1016/j.enpol.2010.03.018, 2010.
692 Parrish, D. D., and Zhu, T.: Clean Air for Megacities, Science, 326, 674-675,
693 doi:10.1126/science.1176064, 2009.
694 Pope, C. A., Ezzati, M., and Dockery, D. W.: Fine-particulate air pollution and life
695 expectancy in the United States, N. Engl. J. Med., 360, 376-386,
696 doi:10.1056/NEJMsa0805646, 2009.
697 Presto, A. A., Gordon, T. D., and Robinson, A. L.: Primary to secondary organic
698 aerosol: evolution of organic emissions from mobile combustion sources, Atmos.
699 Chem. Phys., 14, 5015-5036, doi:10.5194/acp-14-5015-2014, 2014.
700 Ramanathan, V., Crutzen, P. J., Kiehl, J. T., and Rosenfeld, D.: Aerosols, climate, and
701 the hydrological cycle, Science, 294, 2119-2124, doi:10.1126/science.1064034,
702 2001.
703 Reff, A., Bhave, P. V., Simon, H., Pace, T. G., Pouliot, G. A., Mobley, J. D., and
704 Houyoux, M.: Emissions inventory of $PM_{2.5}$ trace elements across the United States,
705 Environ. Sci. Technol., 43, 5790-5796, doi:10.1021/es802930x, 2009.
706 Robinson, A. L., Donahue, N. M., Shrivastava, M. K., Weitkamp, E. A., Sage, A. M.,
707 Grieshop, A. P., Lane, T. E., Pierce, J. R., and Pandis, S. N.: Rethinking organic

708 aerosols: semivolatile emissions and photochemical aging, Science, 315,
709 1259-1262, doi:10.1126/science.1133061, 2007.
710 RÖnkkÖ, T., Virtanen, A., Kannosto, J., Keskinen, J., Lappi, M., and Pirjola, L.:
711 Nucleation mode particles with a nonvolatile core in the exhaust of a heavy duty
712 diesel vehicle, Environ. Sci. Technol., 41, 6384-6389, doi:10.1021/es0705339,
713 2007.
714 Sage, A. M., Weitkamp, E. A., Robinson, A. L., and Donahue, N. M.: Evolving mass
715 spectra of the oxidized component of organic aerosol: results from aerosol mass
716 spectrometer analyses of aged diesel emissions, Atmos. Chem. Phys., 8, 1139-1152,
717 2008.
718 Song, C., Na, K., Warren, B., Malloy, Q., and Cocker, D. R., III: Impact of propene on
719 secondary organic aerosol formation from m-xylene, Environ. Sci. Technol., 41,
720 6990-6995, doi:10.1021/es062279a, 2007a.
721 Song, Y., Xie, S., Zhang, Y., Zeng, L., Salmon, L. G., and Zheng, M.: Source
722 apportionment of $PM_{2.5}$ in Beijing using principal component analysis/absolute
723 principal component scores and UNMIX, Sci. Total Environ., 372, 278-286,
724 doi:10.1016/j.scitotenv.2006.08.041, 2006a.
725 Song, Y., Zhang, Y. H., Xie, S. D., Zeng, L. M., Zheng, M., Salmon, L. G., Shao, M.,
726 and Slanina, S.: Source apportionment of $PM_{2.5}$ in Beijing by positive matrix
727 factorization, Atmos. Environ., 40, 1526-1537, doi:10.1016/j.atmosenv.2005.10.039,
728 2006b.
729 Song, Y., Tang, X., Xie, S., Zhang, Y., Wei, Y., Zhang, M., Zeng, L., and Lu, S.:

730 Source apportionment of $PM_{2.5}$ in Beijing in 2004, J. Hazard. Mater., 146, 124-130,
731 doi:10.1016/j.jhazmat.2006.11.058, 2007b.
732 Stone, E. A., Snyder, D. C., Sheesley, R. J., Sullivan, A. P., Weber, R. J., and Schauer,
733 J. J.: Source apportionment of fine organic aerosol in Mexico City during the
734 MILAGRO experiment 2006, Atmos. Chem. Phys., 8, 1249-1259,
735 doi:10.5194/acp-8-1249-2008, 2008.
736 Ulbrich, I. M., Canagaratna, M. R., Zhang, Q., Worsnop, D. R., and Jimenez, J. L.:
737 Interpretation of organic components from Positive Matrix Factorization of aerosol
738 mass spectrometric data, Atmos. Chem. Phys., 9, 2891-2918,
739 doi:10.5194/acp-9-2891-2009, 2009.
740 Volkamer, R., Jimenez, J. L., San Martini, F., Dzepina, K., Zhang, Q., Salcedo, D.,
741 Molina, L. T., Worsnop, D. R., and Molina, M. J.: Secondary organic aerosol
742 formation from anthropogenic air pollution: Rapid and higher than expected,
743 Geophys. Res. Lett., 33, L17811, doi:10.1029/2006GL026899, 2006.
744 Volkamer, R., Ziemann, P. J., and Molina, M. J.: Secondary Organic Aerosol
745 Formation from Acetylene (C_2H_2)：seed effect on SOA yields due to organic
746 photochemistry in the aerosol aqueous phase, Atmos. Chem. Phys., 9, 1907-1928,
747 2009.
748 Wang, H., Fu, L., Zhou, Y., Du, X., and Ge, W.: Trends in vehicular emissions in
749 China's mega cities from 1995 to 2005, Environ. Pollut., 158, 394-400,
750 doi:10.1016/j.envpol.2009.09.002, 2010.
751 Wang, X., Liu, T., Bernard, F., Ding, X., Wen, S., Zhang, Y., Zhang, Z., He, Q., Lu, S.,

752 Chen, J., Saunders, S., and Yu, J.: Design and characterization of a smog chamber
753 for studying gas-phase chemical mechanisms and aerosol formation, Atmos. Meas.
754 Tech., 7, 301-313, doi:10.5194/amt-7-301-2014, 2014a.
755 Wang, Y., Wang, M., Zhang, R., Ghan, S. J., Lin, Y., Hu, J., Pan, B., Levy, M., Jiang, J.
756 H., and Molina, M. J.: Assessing the effects of anthropogenic aerosols on Pacific
757 storm track using a multiscale global climate model, Proc. Natl. Acad. Sci. USA,
758 111, 6894-6899, doi:10.1073/pnas.1403364111, 2014b.
759 Weitkamp, E. A., Sage, A. M., Pierce, J. R., Donahue, N. M., and Robinson, A. L.:
760 Organic aerosol formation from photochemical oxidation of diesel exhaust in a
761 smog chamber, Environ. Sci. Technol., 41, 6969-6975, doi:10.1021/es070193r,
762 2007.
763 Wu, S., Deng, F., Wei, H., Huang, J., Wang, X., Hao, Y., Zheng, C., Qin, Y., Lv, H.,
764 Shima, M., and Guo, X.: Association of cardiopulmonary health effects with
765 source-appointed ambient fine particulate in Beijing, China: a combined analysis
766 from the Healthy Volunteer Natural Relocation (HVNR) study, Environ. Sci.
767 Technol., 48, 3438-3448, doi:10.1021/es404778w, 2014.
768 Xu, H., Wang, X., Pöschl, U., Feng, S., Wu, D., Yang, L., Li, S., Song, W., Sheng, G.,
769 Fu, J.: Genotoxicity of total and fractionated extractable organic matter in fine air
770 particulate matter in urban Guangzhou: comparison between haze and nonhaze
771 episodes, Environ. Toxicol. Chem., 27, 206-212, doi:10.1897/07-095.1, 2008.
772 Yanowitz, J., McCormick, R. L., and Graboski, M. S.: In-use emissions from
773 heavy-duty diesel vehicles, Environ. Sci. Technol., 34, 729-740,

774 doi:10.1021/es990903w, 2000.
775 Yi, Z., Wang, X., Sheng, G., Zhang, D., Zhou, G., and Fu, J.: Soil uptake of carbonyl
776 sulfide in subtropical forests with different successional stages in south China, J.
777 Geophys. Res., 112, D08302, doi:10.1029/2006JD008048, 2007.
778 Yue, X., Wu, Y., Hao, J., Pang, Y., Ma, Y., Li, Y., Li, B., and Bao, X.: Fuel quality
779 management versus vehicle emission control in China, status quo and future
780 perspectives, Energy Policy, 79, 87-98, 2015.
781 Zhang, K., Hu, J., Gao, S., Liu, Y., Huang, X., and Bao, X.: Sulfur content of gasoline
782 and diesel fuels in northern China, Energy Policy, 38, 2934-2940,
783 doi:10.1016/j.enpol.2010.01.030, 2010.
784 Zhang, Q., Streets, D. G., Carmichael, G. R., He, K. B., Huo, H., Kannari, A.,
785 Klimont, Z., Park, I. S., Reddy, S., Fu, J. S., Chen, D., Duan, L., Lei, Y., Wang, L.
786 T., and Yao, Z. L.: Asian emissions in 2006 for the NASA INTEX-B mission,
787 Atmos. Chem. Phys., 9, 5131-5153, 2009.
788 Zhang, R., Jing, J., Tao, J., Hsu, S. C., Wang, G., Cao, J., Lee, C. S. L., Zhu, L., Chen,
789 Z., Zhao, Y., and Shen, Z.: Chemical characterization and source apportionment of
790 $PM_{2.5}$ in Beijing: seasonal perspective, Atmos. Chem. Phys., 13, 7053-7074,
791 doi:10.5194/acp-13-7053-2013, 2013.
792 Zhang, Y., Wang, X., Blake, D. R., Li, L., Zhang, Z., Wang, S., Guo, H., Lee, F. S. C.,
793 Gao, B., Chan, L., Wu, D., and Rowland, F. S.: Aromatic hydrocarbons as ozone
794 precursors before and after outbreak of the 2008 financial crisis in the Pearl River
795 Delta region, south China, J. Geophys. Res., 117, D15306,

796 doi:10.1029/2011JD017356, 2012.
797 Zhang, Y., Wang, X., Wen, S., Herrmann, H., Yang, W., Huang, X., Zhang, Z., Huang,
798 Z., He, Q., and George, C.: On-road vehicle emissions of glyoxal and
799 methylglyoxal from tunnel tests in urban Guangzhou, China, Atmos. Environ., 127,
800 55-60, doi:10.1016/j.atmosenv.2015.12.017, 2016.
801 Zhao, L., Wang, X., He, Q., Wang, H., Sheng, G., Chan, L., Fu, J., Blake, D.R:
802 Exposure to hazardous volatile organic compounds, PM_{10} and CO while walking
803 along streets in urban Guangzhou, China, Atmo. Environ., 38, 6177-6184,
804 doi:10.1016/j.atmosenv.2004.07.025, 2004
805 Zheng, M., Salmon, L. G., Schauer, J. J., Zeng, L. M., Kiang, C. S., Zhang, Y. H., and
806 Cass, G. R.: Seasonal trends in $PM_{2.5}$ source contributions in Beijing, China, Atmos.
807 Environ., 39, 3967-3976, doi:10.1016/j.atmosenv.2005.03.036, 2005.

808
809

Table 1 Information of three diesel vehicles used in the experiments

Vehicle ID	Vehicle type	Emission standard	Model year	Mileage (km)	Displacement (cm^{-3})	Power (kW)	Weight (kg)
Foton	MDDV	Euro III	2011	16,000	2,499	65	2,580
Changan	MDDV	Euro III	2013	15,000	2,540	67	3,775
JAC	HDDV	Euro III	2013	11,000	9,839	215	24,900

Table 2 Summary of the results for the diesel vehicle experiments

Expt. No.	Vehicle	T (°C)	RH (%)	NO [a] (ppbv)	NO_2 [a] (ppbv)	propene (ppmv)	dilution ratio	OH ($\times 10^6$ molecules cm^{-3})	EF_{BC} (g kg^{-1} fuel)	EF_{POA} (g kg^{-1} fuel)	PF_{SOA} (g kg^{-1} fuel)		O/C		H/C		OM/OC	
											ω=0	ω=1	ini[b]	fin[c]	ini[b]	fin[c]	ini[b]	fin[c]
1	JAC	24.2	2.3	3246	220	3.81	71	3.11	0.16	0.19	0.30	0.61	0.31	0.45	1.48	1.34	1.52	1.70
2	Foton	24.9	2.5	1156	144	1.57	136	1.74	0.19	0.34	0.26	0.56	0.11	0.17	1.81	1.71	1.33	1.40
3	Foton	24.1	1.5	1185	136	1.66	115	5.23	0.18	0.28	0.28	0.68	0.16	0.30	1.70	1.62	1.36	1.55
4	Foton	24.9	2.7	749	153	0.95	213	5.00	0.19	0.32	0.34	0.76	0.39	0.45	1.44	1.36	1.68	1.75
5	Foton	25.2	54	2151	236	3.09	66	2.24	0.15	0.18	0.23	0.60	0.39	0.66	1.53	1.31	1.64	2.04
6	Changan	24.7	2.5	733	248	1.17	210	3.99	0.47	0.91	0.62	1.8	0.50	0.66	1.40	1.37	1.80	2.02
7	Changan	24.5	1.7	1113	43	0.01	214	4.23	0.50	0.74	0.39	0.50	0.34	0.51	1.41	1.39	1.75	1.82
8	Changan	24.6	54	1286	205	2.04	188	4.10	0.51	0.72	0.57	1.1	0.26	0.47	1.51	1.43	1.48	1.76

[a]. values before adding HONO.

[b]. initial value, the value before turned on the lights.

[c]. final value, the value after 5 hours photo-oxidation.

818 **Table 3** The predicted SOA production from each aromatic hydrocarbons (measured

819 by PTR-MS) in all experiments.

Expt.	Predicted SOA (μg m^{-3})					Predicted SOA/
No.	Benzene	Toluene	C_2-benzene	C_3-benzene	C_4-benzene	Measured SOA [a]
1	0.015	0.019	0.022	0.081	0.085	1.7%
2	0.202	0.028	0.050	0.068	0.114	2.1%
3	0.069	0.013	0.051	0.054	0.068	1.0%
4	0.127	0.055	0.013	0.007	0.017	0.6%
5	0.074	0.012	0.082	0.075	0.108	1.0%
6	0.237	0.213	0.496	0.018	0.007	2.8%
7	0.164	0.065	0.014	0.052	0.077	1.0%
8	0.329	0.072	0.067	0.124	0.229	1.6%

820 [a]. measured SOA were wall loss corrected at $\omega = 0$.

821

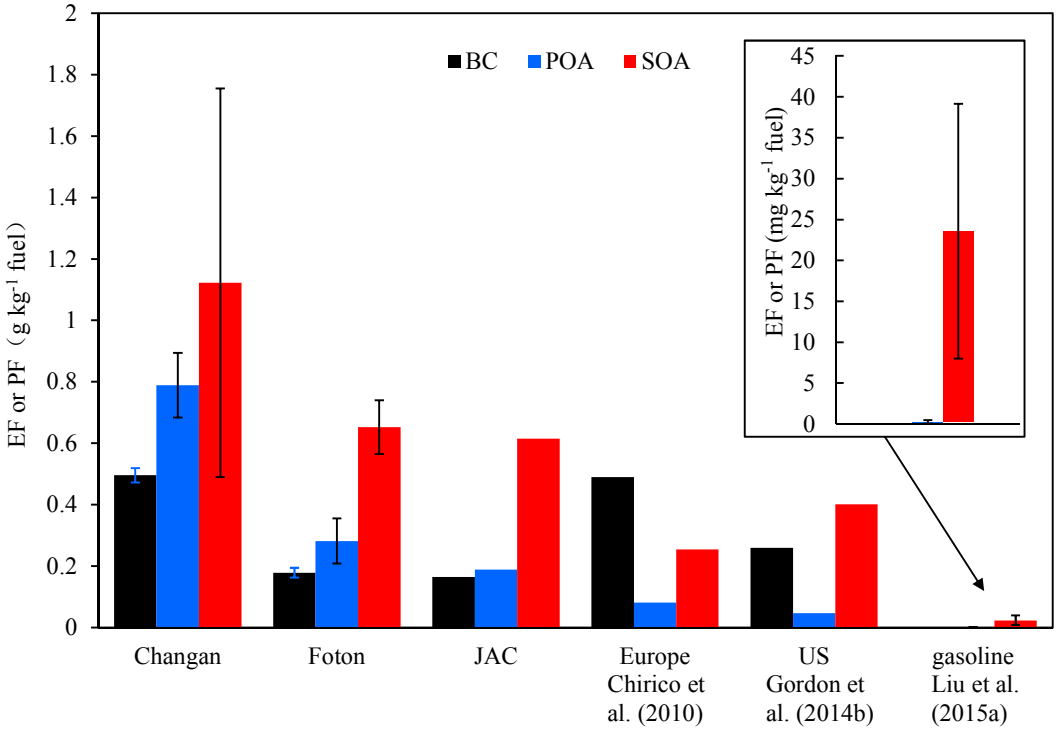

822

823 **Figure 1** Emission factors of BC and POA and production factors of SOA for ω=1
824 from different diesel vehicle exhausts in this study, as well as those from diesel and
825 gasoline vehicle reported in literatures. The error bars represent the ranges of EFs and
826 PFs for each vehicle. The emission factor reported by Chirico et al. (2010) is under
827 idling condition for a MDDV without aftertreatment. The emission factor reported by
828 Gordon et al. (2014b) is the result under creep + idling condition for a HDDV without
829 aftertreatment. The emission factor of gasoline is from the dataset of Liu et al. (2015a),
830 and BC was not reported but comparatively negligible. The right-hand side of the
831 figure shows average values from 5 gasoline vehicle experiments from Liu et al.
832 (2015a)

833

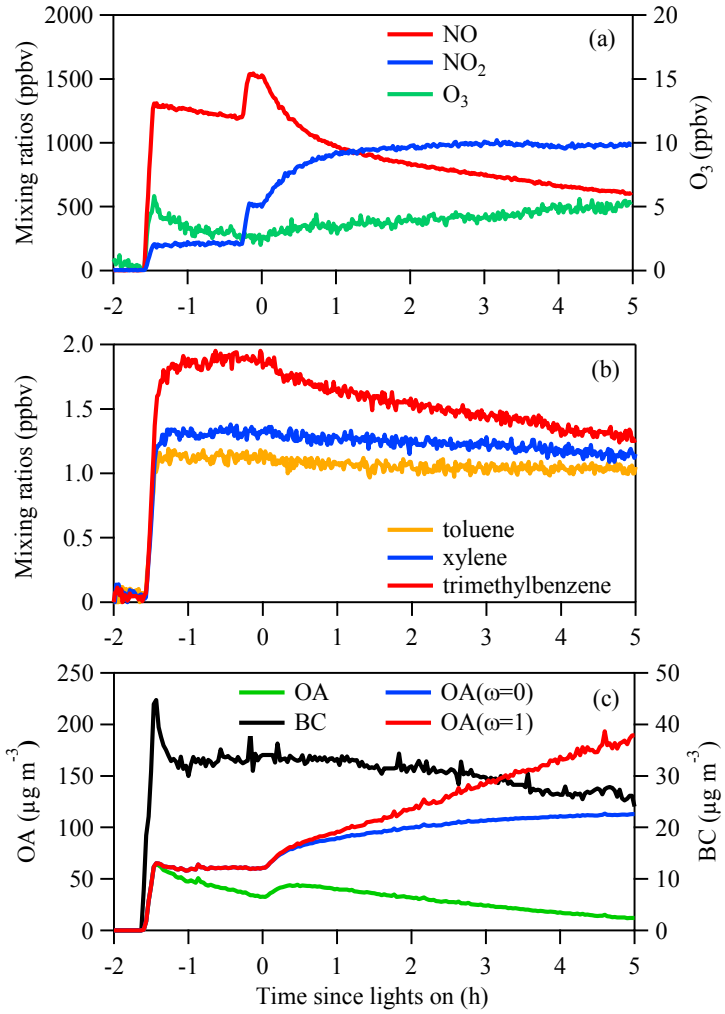

834

835 **Figure 2** Evolution of gaseous and particulate species during a typical smog chamber

836 experiment (Experiment 8). Concentrations of (a) NO_x, O_3, (b) single-ring aromatic

837 SOA precursors, and (c) measured OA and BC and wall loss corrected organic aerosol

838 (OA(ω=0) and OA(ω=1)). t=0 represents the time we turned on the black lights.

839

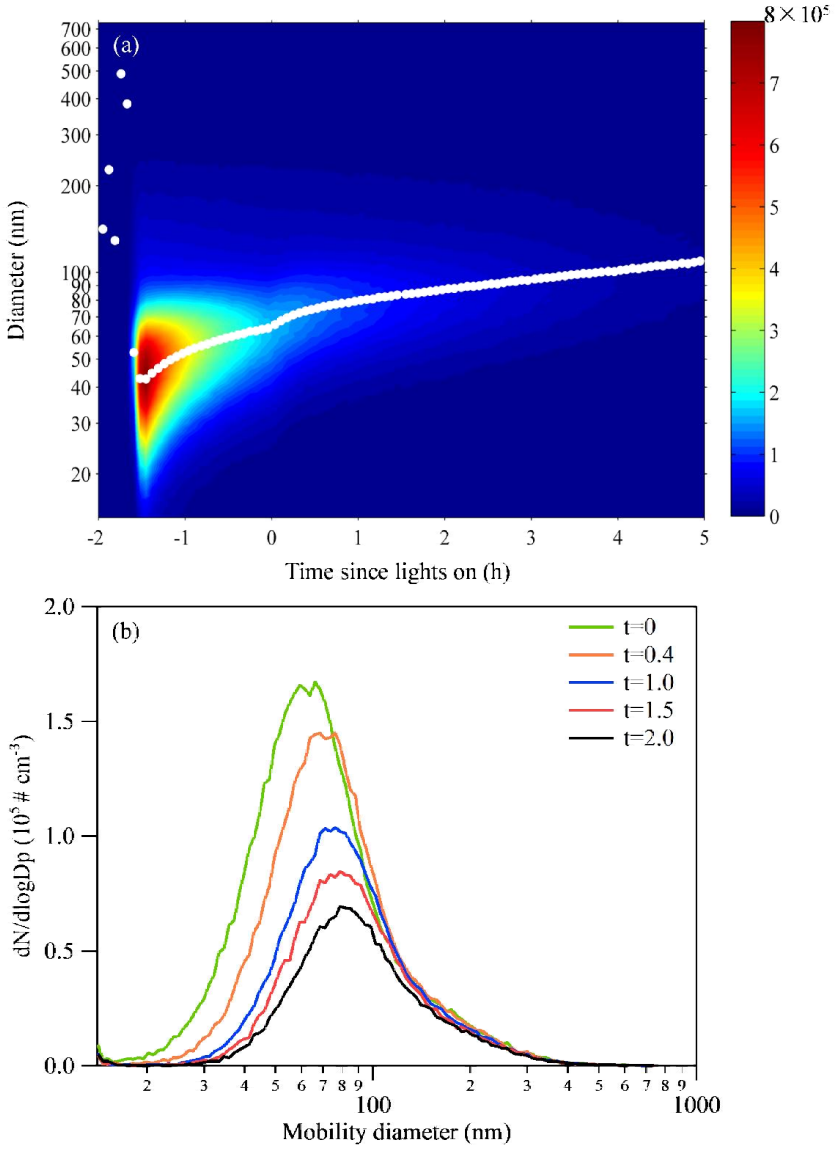

840

841 **Figure 3** (a) Particle size–number concentration distributions as a function of time.
842 The white dots represent the evolution of median diameter during the experiment. (b)
843 Particle number distribution in Experiment 8 at t=0 h, 0.4 h, 1 h 1.5 h and 2 h after
844 lights were turned on.

845

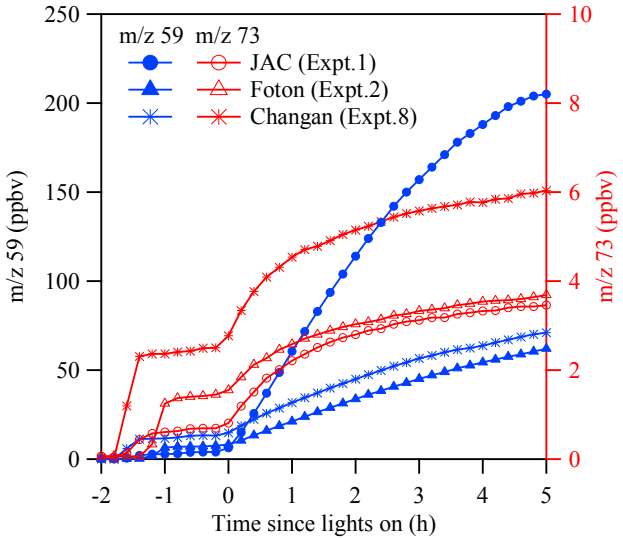

846

847 **Figure 4** The mixing ratios of ions at *m/z* 59 (left axis) and *m/z* 73 (right axis)

848 measured by PTR-MS during chamber experiment. Blue color is the mixing ratios of

849 *m/z* 59, red color is *m/z* 73. Circle represent for experiment 1, triangle represent for

850 experiment 2, asterisk represent for experiment 8.

851

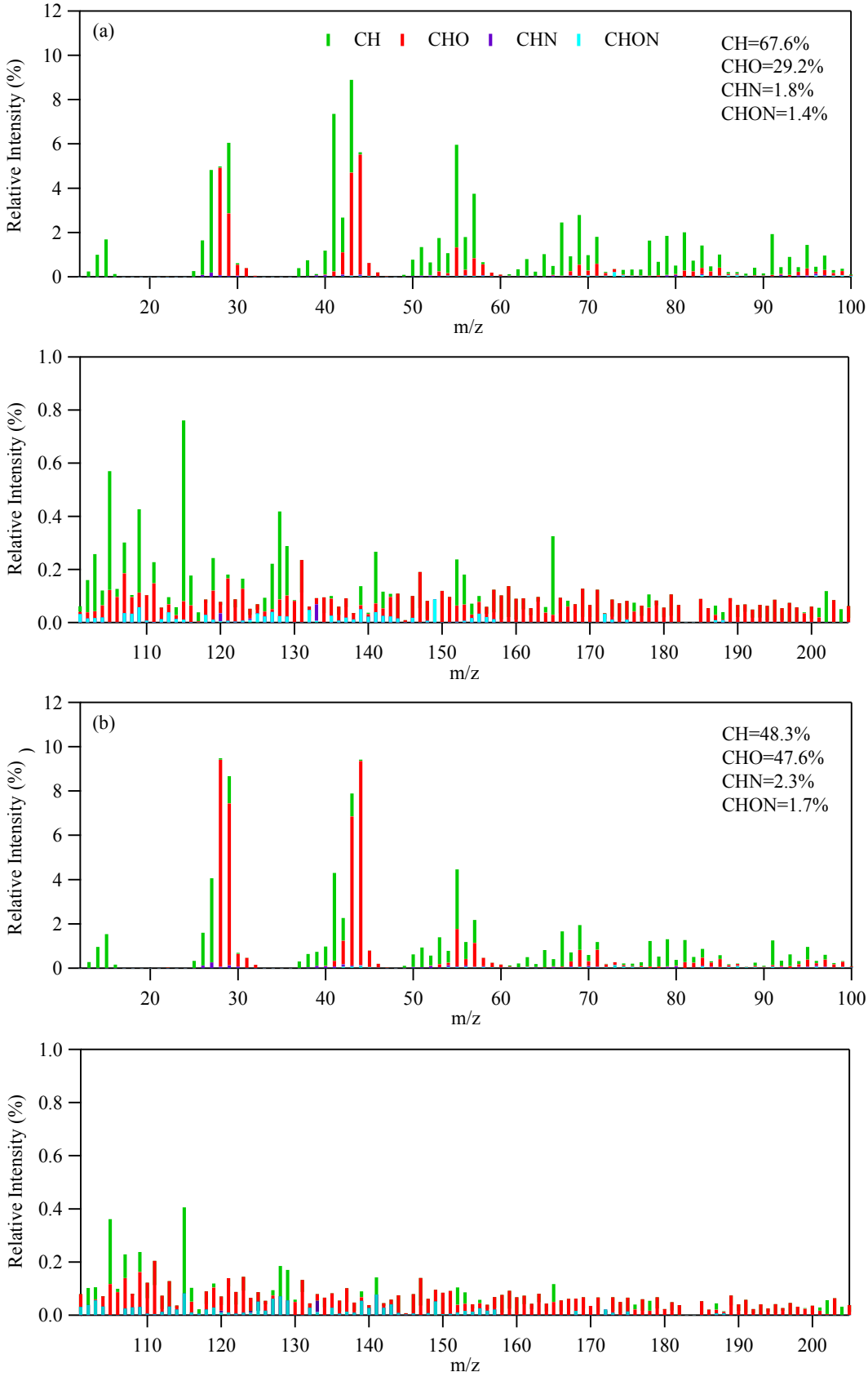

852

853 **Figure 5** Average mass spectra in high resolution (normalized to the total organic

mass) of POA and OA after 5-hour aging measured by AMS in Experiment 8. (a) The average mass spectra of POA. (b) The average mass spectra of OA after 5 hours photo-oxidation.

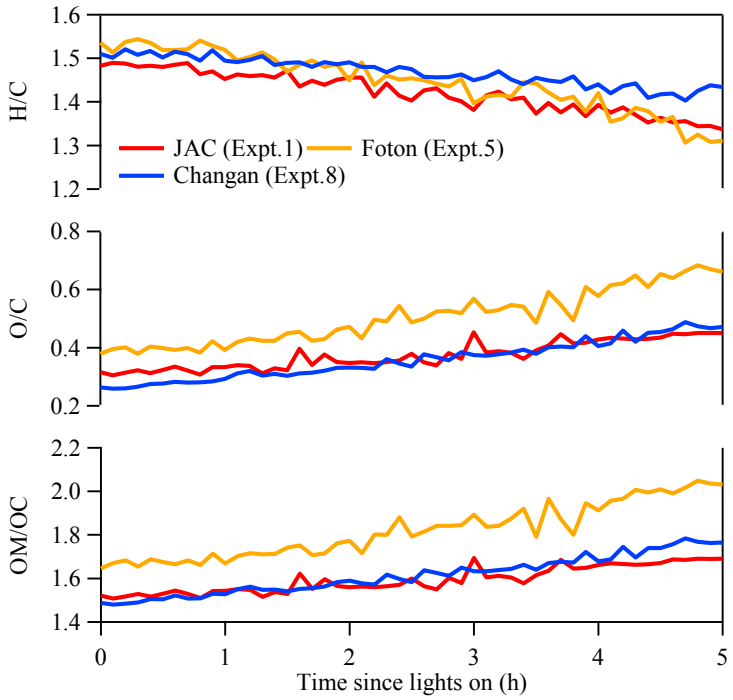

858

859 **Figure 6** Time series of O/H and O/C atomic ratios and average OM/OC ratios during

860 chamber experiments.

861

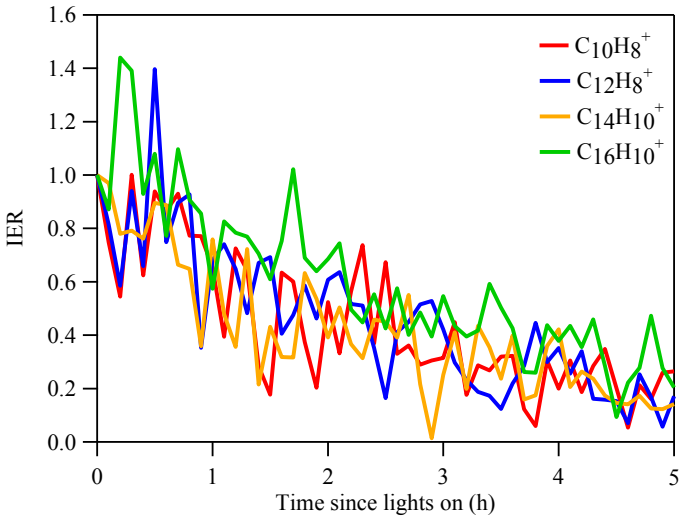

862

863 **Figure 7** Evolution of the ion enhancement ratios (IERs) of PAHs signals during

864 Experiment 8.

865

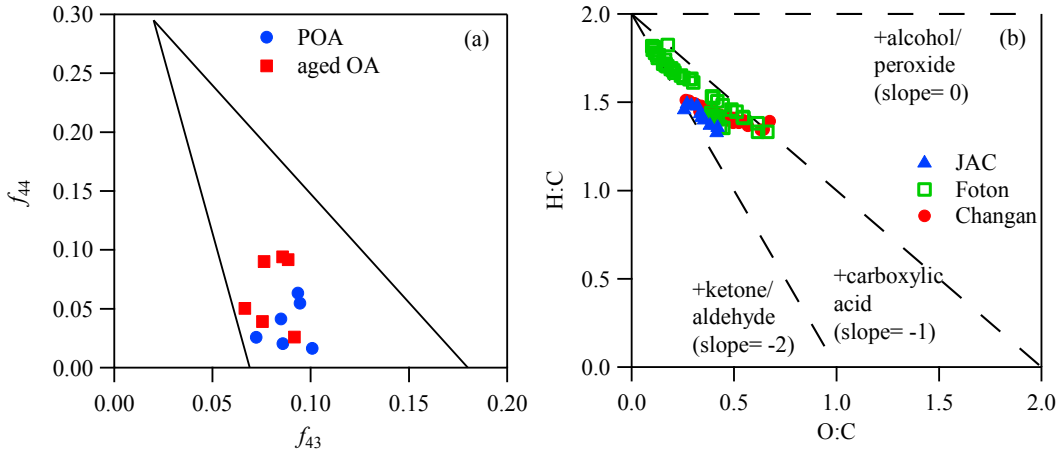

866

867 **Figure 8** (a) The fractions of total organic signal at *m/z* 43 (f_{43}) versus *m/z* 44 (f_{44}) for
868 POA and 5 hours aged OA. The solid lines define the space where ambient OOA
869 components fall. (b) The van Krevelen plot of all experiments. Dotted lines show
870 slops of 0, -1 and -2. Solid triangle represents the experiment for JAC, open square
871 represents the experiments for Foton, solid circle represent the experiments for
872 Changan.